

Numerical Simulation of Flows around Broad-leaf Trees

Fuh-Min Fang^{1*}, Yi-Chao Li² and Cheng-Yang Chung³

¹*Department of Civil Engineering, National Chung Hsing University,
Taichung, Taiwan 402, R.O.C.*

²*Wind Engineering Research Center, Tamkang University,
Tamsui, Taiwan 251, R.O.C.*

³*Architecture and Building Research Institute, Ministry of Interior,
New Taipei City, Taiwan 231, R.O.C.*

Abstract

A numerical model was established to predict flow past discrete broad-leaf trees so as to provide a handy tool for pedestrian wind analysis during the preliminary design stage for local wind environments. In the study, a tree factor was proposed to reflect the effect due to the existence of the trees. Besides the applications of numerical computations in flow analysis, wind tunnel measurements were also performed to guide and confirm the numerical simulations. Results showed that the calibrated tree factor generally increased with increases of the volume ratio and horizontal thickness of the tree body. Based on the calibrated relationship of the tree factor, finally, additional numerical computations were performed to simulate flow past an isolated tree and dual trees in a tandem and a side-by-side arrangement. The predicted downstream wind velocity profiles appeared in good agreements with the measurement results.

Key Words: Large Eddy Simulation, Wind Tunnel Test, Bluff-body Flow, Porous Body

1. Introduction

Planting trees in building areas can not only upgrade the local landscape but to some extent improve the wind environment, particularly regarding the reduction of wind speed in the pedestrian level. Therefore, how to analyze the wind flow in areas with trees becomes an important task for the designers during the planning stage. Commonly, wind tunnel experiments can be employed to analyze the wind flow problem. Besides the amount of human labor and time required in the experimental work, technical difficulties (such as the scale effect) are generally encountered. On the other hand, numerical simulations can be another alternative for the analysis.

The flow pattern around a tree may appear somewhat

different from that around an impermeable solid body due to its porous nature. As a part of fluid penetrates the tree, the shedding vortices can interact with the penetrating flow and disturb the formation of the downstream wake. Physically, this extent of the interaction effect may depend on the porosity and thickness of the tree.

The goal of the study is to establish a numerical model, capable of correctly predicting flows past discrete broad-leaf trees so as to provide a handy tool for pedestrian wind analysis during the preliminary design for local wind environments. Besides numerical computations, wind tunnel measurements were also performed to guide and confirm the numerical simulations.

2. Related Studies

Most of the previous related work concentrated on

*Corresponding author. E-mail: fmfang@nchu.edu.tw

the studies in the research areas of forestry and meteorology. The main focus was to investigate the overall wind flow characteristics around group trees in forest territories. Based on a global approach, the three-dimensional wind flow analyses were generally simplified into a two- or one-dimensional problem depending on the spatial distributions of local group trees. Typically, Finnigan [1] stated that the surface wind flow region could be divided into a canopy and a surface sublayer. By field investigations, Raupach et al. [2] indicated that the pattern of turbulent flow characteristics within the canopy sublayer was close to that of a mixing-layer flow. A description of wind speed profile was also proposed by Raupach et al. [3] based on wind tunnel results. Similar profiles in forest territories were also brought out by Mihailovic et al. [4]. Based on wind tunnel results, Massman [5] proposed a leaf area index (LAI) and discussed its influence on the associated wind speed profiles, surface shear velocities and roughness heights. Additionally, Novak et al. [6] found that a change of the spatial density of trees in a forest could affect the local mean and turbulent flow characteristics, mainly dominated by large-scale turbulence eddies. Further results of wind tunnel experiments regarding wind flows past a single layer and a double layer of plants by Boldes et al. [7] revealed that mixing flows occurred in the wake region and produced bleed flows due to the effect of large-scale eddies. Moreover, Flesch and Wilson [8,9] carried out wind tunnel experiments to investigate the protected area as well as the extent of wind speed reduction downstream of group trees.

There are also several studies related to wind flows around trees by using numerical analysis. Typically, Shaw and Schumann [10] proposed an inclusion of a source term in the momentum equations to physically reflect the tree effects. The introduced drag term was the product of the drag coefficient, leaf density and combined velocity. Wilson and Flesch [11] used a two-dimensional numerical model to simulate flows past forests. The predicted wind speed profiles were in good agreements with the in-field results. By performing large eddy simulations, Su et al. [12] predicted neutrally stratified flows past

forests. Patton and Davis [13] also carried out large eddy simulations to investigate the dispersion mechanism of chemicals in forests. Watanabe [14] performed large eddy computations to examine the turbulence structure above forests. Moreover, Sládek et al. [15] investigated numerically the two- and three-dimensional wind fields of boundary-layer flows past forests in complicated land territories.

3. Numerical Method

A weakly-compressible-flow method [16] is adopted in the flow calculations. The original form of the method is applicable to inviscid flow cases and is further extended to viscous turbulent flow simulations. Under a barotropic assumption (density is a function of pressures only), for low-mach-number flows the continuity and momentum equations in index forms can be approximated as [16]

$$\frac{\partial p}{\partial t} + \frac{\partial}{\partial x_j}(Ku_j) = 0 \quad (1)$$

$$\frac{\partial u_i}{\partial t} + \frac{\partial u_i u_j}{\partial x_j} = -\frac{1}{\rho} \frac{\partial p}{\partial x_i} + \nu \frac{\partial^2 u_i}{\partial x_j x_j} \quad (2)$$

where $K (= \rho c^2)$ is the bulk modulus of elasticity; ρ , p and c are respectively density, pressure and sound speed.

For turbulent flows, a large eddy simulation approach is applied. Accordingly, any quantity, g , can be decomposed into resolvable-scale and subgrid-scale components as

$$g = \bar{g} + g' \quad (3)$$

Through a space-averaging process, the governing equations become

$$\frac{\partial \bar{p}}{\partial t} + \frac{\partial}{\partial x_j}(K\bar{u}_j) = 0 \quad (4)$$

$$\begin{aligned} \frac{\partial \bar{u}_i}{\partial t} + \frac{\partial \bar{u}_i \bar{u}_j}{\partial x_j} = & -\frac{\partial (\bar{p}/\rho)}{\partial x_i} \\ & + \frac{\partial}{\partial x_j} \left[-\overline{u'_i u'_j} - \overline{u'_i \bar{u}_j} - \overline{\bar{u}_i u'_j} - (\overline{\bar{u}_i \bar{u}_j} - \bar{u}_i \bar{u}_j) \right] + \nu \frac{\partial \bar{u}_i}{\partial x_j} \end{aligned} \quad (5)$$

By adopting Reynold's averaging assumption as

$$\overline{u_i u_j} - \overline{u_i} \overline{u_j} + (\overline{u_i u_j} - \overline{u_i} \overline{u_j}) = 0 \quad (6)$$

one obtains

$$\frac{\partial \overline{u_i}}{\partial t} + \frac{\partial \overline{u_i u_j}}{\partial x_j} = -\frac{\partial(\overline{p^* / \rho})}{\partial x_i} + \frac{\partial}{\partial x_j} \left[-\overline{u_i u_j} - \frac{1}{3} \overline{u_i u_j} \delta_{ij} \right] + \nu \frac{\partial \overline{u_i}}{\partial x_j} \quad (7)$$

where δ_{ij} is the Kronecker delta function and $p^* = p + (\rho/3) \overline{u_i u_i}$.

As the subgrid-scale stress terms are modeled by

$$-\overline{u_i u_j} - \frac{1}{3} \overline{u_i u_j} \delta_{ij} = \nu_t S_{ij} \quad (8)$$

where

$$S_{ij} = \left(\frac{\partial \overline{u_j}}{\partial x_i} + \frac{\partial \overline{u_i}}{\partial x_j} \right) \quad (9)$$

Eq. (7) becomes

$$\frac{\partial \overline{u_i}}{\partial t} + \frac{\partial \overline{u_i u_j}}{\partial x_j} = -\frac{\partial(\overline{p^* / \rho})}{\partial x_i} + \frac{\partial}{\partial x_j} [\tau_{ij}] \quad (10)$$

where τ_{ij} is the combination of the viscous and the subgrid-scale stress term, in which the subgrid-scale diffusion coefficient is expressed in the form suggested by Smagorinsky [17] as

$$\nu_t = (C_s \Delta)^2 \sqrt{\frac{S_{ij}^2}{2}} \quad (11)$$

where Δ is the characteristic length of the computational cell and C_s is the Smagorinsky constant.

In the flow computations, a finite-volume approach is employed to obtain the solutions of Eqs. (7) and (10) for spatial volumes wholly occupied by air. For the computational cells containing leaves and twigs, on the other hand, the momentum equation is modified by adding a source term proposed by Shaw and Schumann [10] as

$$\frac{\partial \overline{u_i}}{\partial t} + \frac{\partial \overline{u_i u_j}}{\partial x_j} = -\frac{\partial(\overline{p^* / \rho})}{\partial x_i} + \frac{\partial}{\partial x_j} [\tau_{ij}] + (f_D)_i \quad (12)$$

with

$$\overline{f_D} = [-C_D a u |\overline{V}|, -C_D a v |\overline{V}|, -C_D a w |\overline{V}|]^T \quad (13)$$

where C_D is the drag coefficient and “ a ” is the leaf surface area per unit volume.

Equations (4) and (10) (or Eq. (12)) can be presented in a conservative form as

$$\frac{\partial G}{\partial t} + \nabla \cdot \overline{F} = 0 \quad (14)$$

The computation can proceed using an integration over a specific control volume (∇) as

$$\int_{\nabla} \frac{\partial G}{\partial t} d\nabla + \int_{\nabla} \nabla \cdot \overline{F} d\nabla = 0 \quad (15)$$

By the divergence theorem, one has

$$\frac{\partial G_m}{\partial t} = -\frac{1}{\nabla} \int_s \tilde{n} \cdot \overline{F} dS \quad (16)$$

where G_m is the mean quantity referred to the center of the volume (computational cell) and \tilde{n} is the normal surface vector. By knowing the G_m quantities of the flow field at a starting time step, the integral form of Eq. (16) can be used to calculate the change of G_m within an elapsed period, Δt , to further update the G_m values for the next time step.

In the computations, appropriate pressure and velocity values are specified at exterior phantom cells outside the boundaries to reflect the correct physical nature of the boundaries. For solid boundaries, a no-slip condition is used. At the upstream section, a prescribed velocity profile is imposed. On the other hand, the average pressure at the downstream end section is set as the reference pressure. On the boundary at the top, the values at the phantom cells are specified according to a zero-gradient assumption in the direction normal to the boundary.

4. Wind Tunnel Experiments

Experiments were conducted at the ABRI (Architecture and Building Research Institute) wind tunnel in Taiwan. The size of the test section is 2.6 m in height and 4.0 m in width. The maximum wind speed in the test sec-

tion is 35 m/s with a turbulent intensity less than 1%. In the experiments, rectangular panels ($D = 0.28$ m and B varies from 0.14 m to 0.56 m), containing a number of parallel and evenly-spaced leaf strings (see Figure 1), were installed horizontally in the direction perpendicular to the uniform approaching flow (see Figure 2; $U_0 = 10$ m/s) at a location near the center of the tunnel cross-section. The size of the leaves is about 0.025 m in width and 0.045 m in length. The Reynolds number ($Re = U_0 D/\nu$; ν is the kinematic viscosity of air) is about 3.83×10^5 . Two vertical plates, with a distance of 0.8 m, were set at the side ends of the panels to produce two-dimensional flow patterns. The corresponding blockage ratio was less than 1%. Hot-film anemometry was adopted to measure the downstream cross-sectional mean and root-mean-square velocity profiles at the center vertical plane. The results would be used to compare with those from the numerical computations.

5. Calibration of Tree Factor

As the factor of leaf surface area per unit volume ("a" value), proposed by Shaw and Schumann [10], cannot not be easily measured technically, a new parameter is proposed in the study, defined as

$$C_{Da} = C_D a \quad (17)$$

To investigate how C_{Da} varied with the conditions of trees, wind tunnel experiments were performed. In the experiments, rectangular panels ($D = 0.28$ m and B varies from 0.14 m to 0.70 m) with various numbers of

broad-leaf strings corresponding to different volumetric tree ratios (γ), defined as the tree volume per unit volume of space, were set in the test section and the downstream mean and root-mean-square velocity profiles were measured at several selected sections ($x_D = 4D, 6D, 8D$ and $10D$). On the other hand, a series of numerical simulations with a number of guessed C_{Da} values were also performed. By comparing with the measurement profiles corresponding to a prescribed thickness (B) and volumetric tree ratio (γ), the C_{Da} value that lead to the best agreement between the measurement and calculated profiles was then obtained. Figures 3 and 4 illustrate typical examples ($B = 1.0D, \gamma = 0.7\%, U_0 = 10$ m/s, $C_{Da} = 3.571$ m⁻¹) of the downstream mean and root-mean-square velocity profile comparisons.

Accordingly, Figure 5 depicts the contour plot of the resulting C_{Da} value in relation to the panel thickness (B) and the volumetric tree ratio (γ). The tendency shows that the C_{Da} value generally increases with an increase of the volumetric tree. When the panel thickness is less than about 0.15 m, C_{Da} increases with an increase of B . As B is greater than about 0.15 m, on the other hand, C_{Da} tends to decrease with an increase of B and the extent of decrease appears more significant when γ increases.

It is noted that the variation of the volumetric tree ratio (γ) should cover the range of general engineering applications regarding coniferous trees. Due to spatial limitations of the wind tunnel tests, however, the resulting C_{Da} variation is valid for B less than 0.70 m.

6. Flow Simulations

Based on the result in Figure 5, simulations were conducted further to examine the validity of the cali-

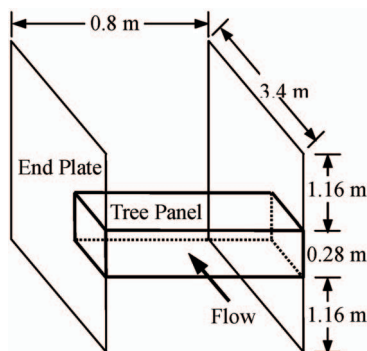


Figure 1. Sketch of experimental set-up.

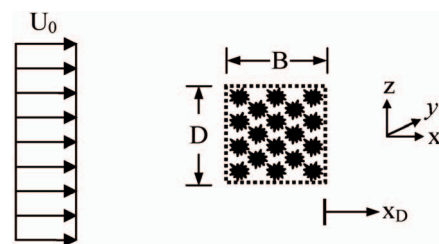


Figure 2. Schematic of wind tunnel experiments.

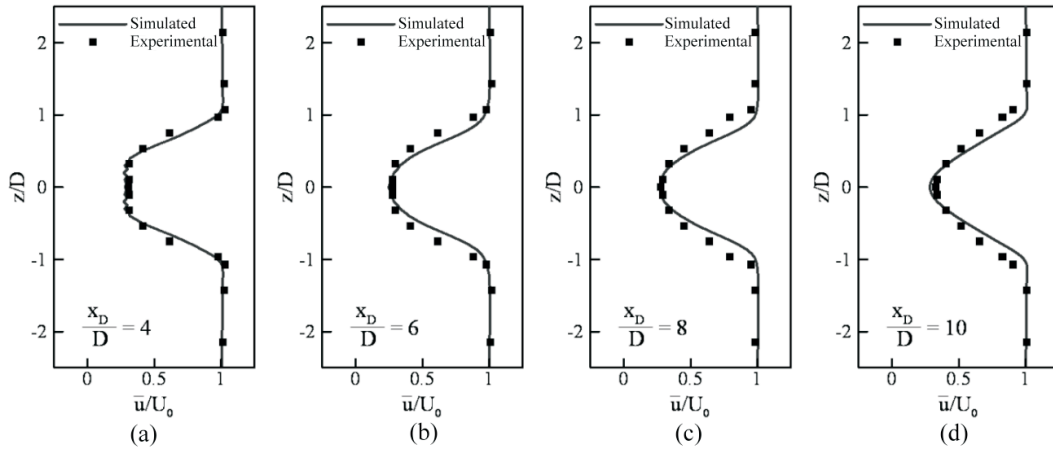


Figure 3. Typical comparison of mean velocity profiles behind the tree panel.

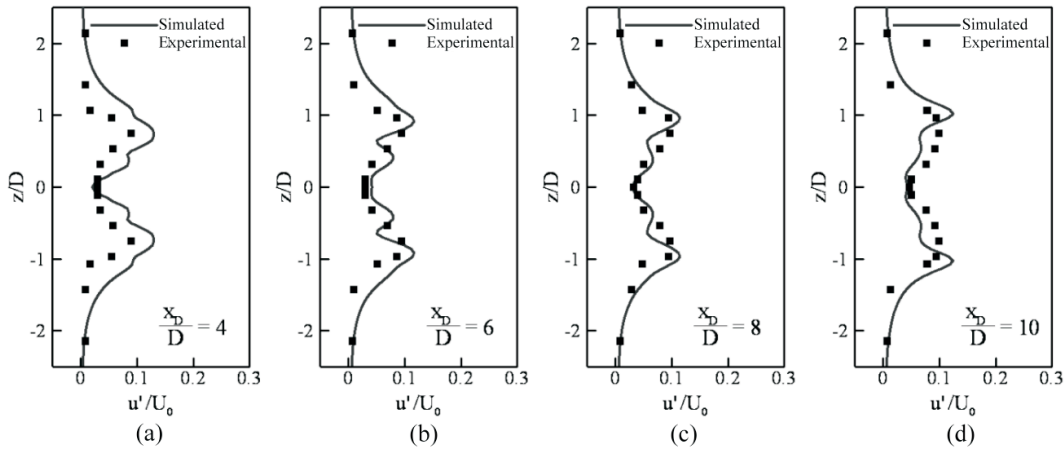


Figure 4. Typical comparison of root-mean-square velocity profiles behind the tree panel.

brated C_{Da} variations. In addition, parallel wind tunnel experiments were also carried out to measure the downstream velocity profiles for comparisons. In all the three-dimensional flow computations, a uniform approaching flow was selected ($U_0 = 10$ m/s). To consider both the accuracy of the flow predictions and the efficiency of the numerical calculations, the vertical size of the computational domain was chosen as $12D$ ($D = 0.28$ m). In the longitudinal direction, the distances from the upstream and downstream end sections to the closest tree edge were respectively $9D$ and $16D$. On the other hand, the transverse distance from the domain sides to the tree edge was $7.5D$. Preliminary test results revealed that the relative error lead by this domain selection is no more than 3%.

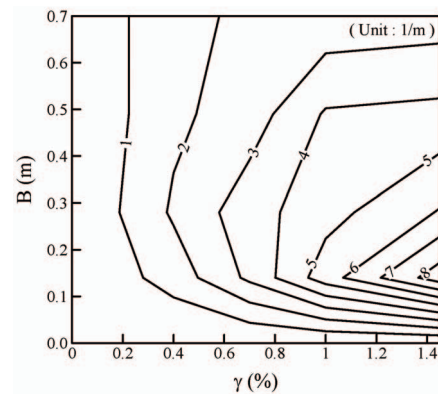


Figure 5. Contours of C_{Da} (in m^{-1}).

6.1 Uniform Flow Past an Isolated Broad-leaf Tree

Figure 6 depicts the schematic of the problem. In the computation, the axisymmetric-shape tree body was di-

vided into several horizontal layers, and the C_{Da} values associated with the grid cells in each layer were taken from the calibration contour plot (Figure 5) according to the corresponding horizontal thickness and volume ratio of the tree body. On the other hand, the main tree trunk, a circular cylinder with a diameter of 0.06 m, was treated as a solid body in the flow simulation.

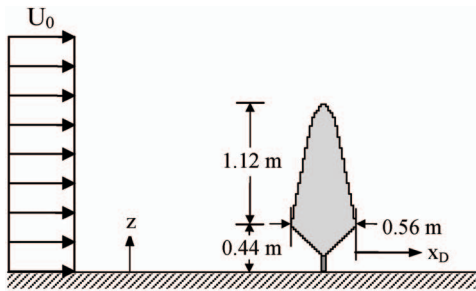


Figure 6. Contours of C_{Da} (in m^{-1}).

The comparisons of normalized mean and root-mean-square velocity profiles at two typical downstream cross-sections at $x_D = 6D$ and $x_D = 8D$ (x_D is the coordinate in the along-wind direction starting from the downstream edge of the tree) are shown in Figures 7 and 8. The spatial correlation coefficient of the cross-sectional velocity variations between the experimental and calculated results are respectively 0.965 and 0.864 as well as 0.965 and 0.878, indicating well predictions of the flows.

6.2 Uniform Flow Past Dualbroad-leaf Trees with a Tandem Arrangement

An additional flow computation was conducted to simulate a uniform flow past dual coniferous trees in a tandem arrangement with an edge-to-edge distance of 0.56 m. The comparisons at two typical cross-sections

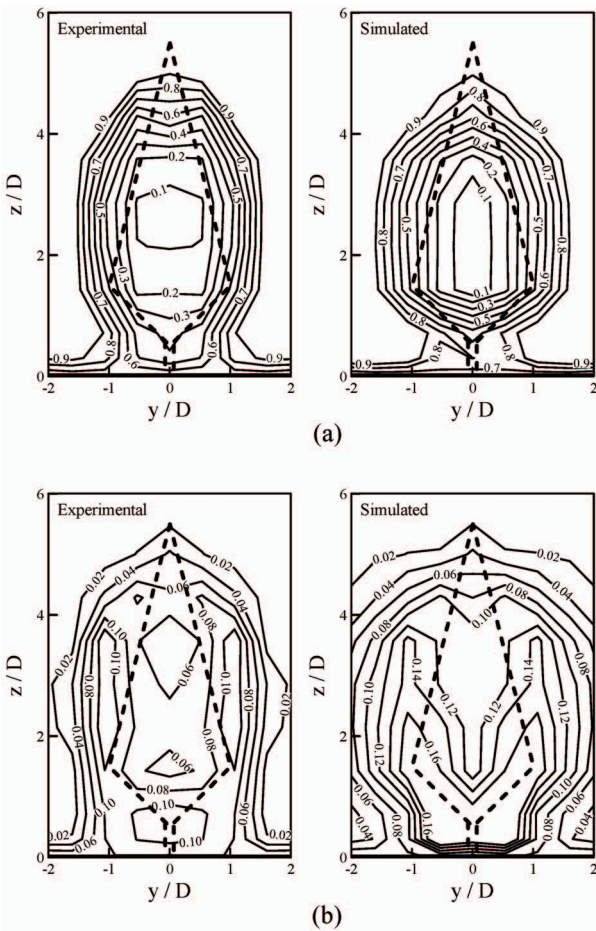


Figure 7. Comparison of mean and rms velocity profiles of an isolated tree ($x_D = 6D$).

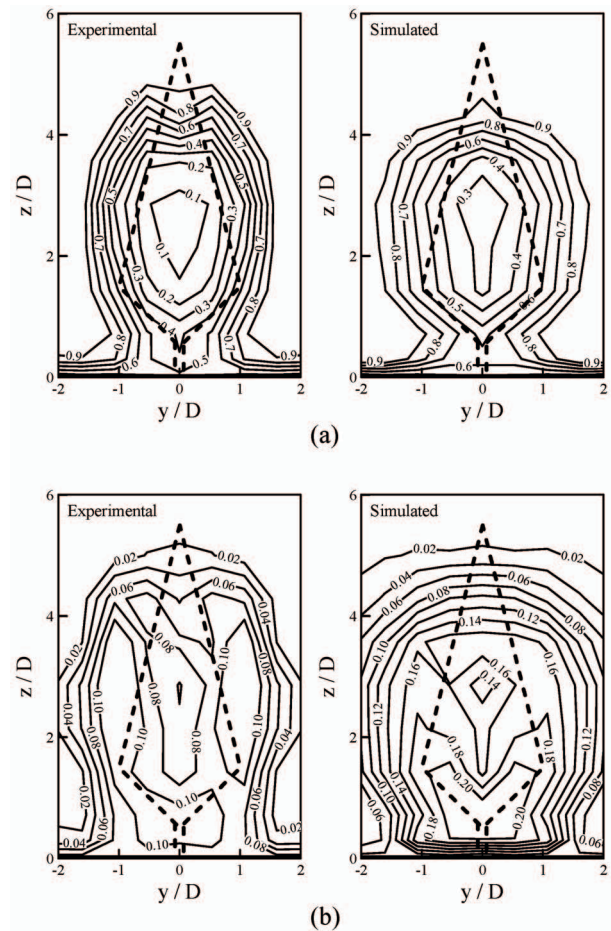


Figure 8. Comparison of mean and rms velocity profiles of an isolated tree ($x_D = 8D$).

($x_D = 6D$ and $x_D = 8D$; x_D is the coordinate in the along-wind direction starting from the trailing edge of the downstream tree) in Figures 9 and 10 show that the agreements between the measurement and the predicted results appear also good. The spatial correlation coefficients of the comparisons are respectively 0.976 and 0.963 for the mean profiles, and 0.949 and 0.915 for the root-mean-square profiles.

6.3 Uniform Flow Past Dualbroad-leaf Trees with a Side-by-side Arrangement

A uniform flow past dual coniferous trees in a side-by-side arrangement with an edge-to-edge transverse distance of 0.14 m was further simulated numerically. The comparisons in Figures 11 and 12 show that at two typical downstream cross-sections ($x_D = 6D$ and $x_D = 8D$), again, the mean and fluctuating velocity profiles are

predicted with acceptable accuracy (correlation coefficients are respectively 0.945 and 0.819 as well as 0.951 and 0.916).

7. Discussion

Generally, analyzing the pedestrian wind flow with discrete trees by numerical simulation is considered more economical, compared to the execution of wind tunnel model experiments. However, if one attempts to simulate the flow with the consideration of all detailed geometries of the trees, an extremely fine numerical grid system is then required and results in a great amount of numerical computation. For practical reasons, Shaw and Schumann [10] proposed the concept of treating the tree body as a porous media. That is, extra source terms are added in the spatial volumes occupied by the tree body. As the

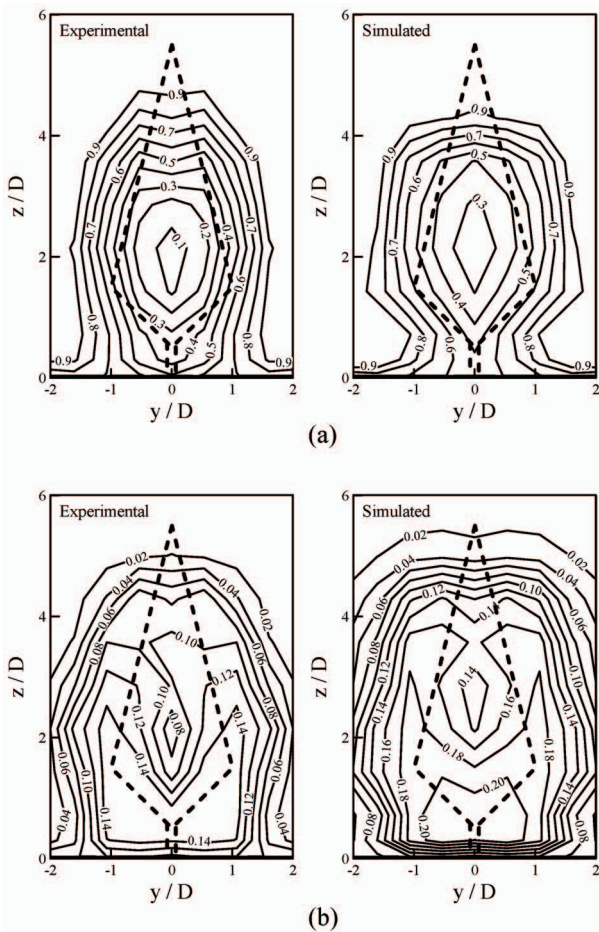


Figure 9. Comparison of velocity profiles of dual trees in a tandem arrangement ($x_D = 6D$).

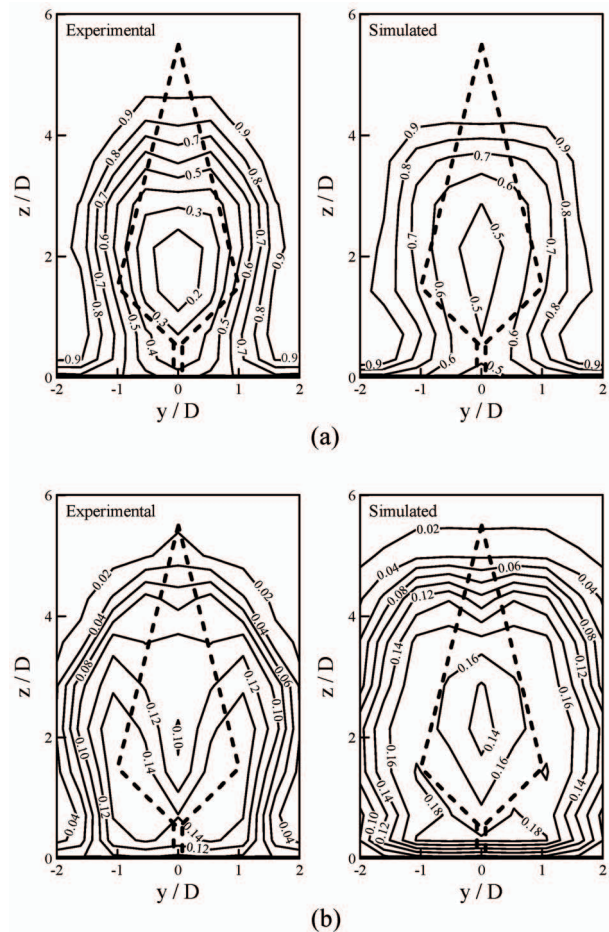


Figure 10. Comparison of velocity profiles of dual trees in a tandem arrangement ($x_D = 8D$).

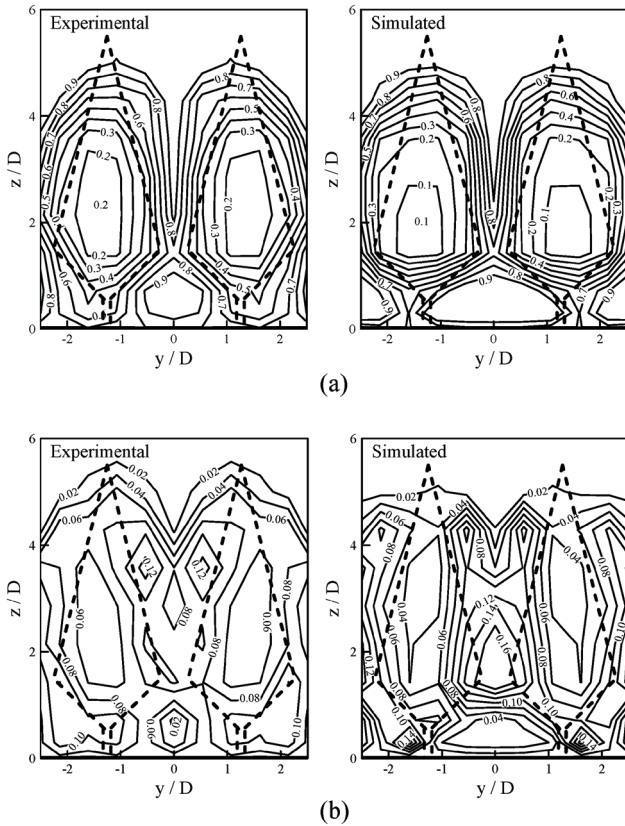


Figure 11. Comparison of velocity profiles of dual trees in a side-by-side arrangement ($x_D = 6D$).

form of the suggested source term (Eq. 13) is examined, it is found that C_D (the drag coefficient) is unknown and depends on the solution of the unsteady flow. Moreover, an accurate estimate of the factor (the leaf surface area per unit volume) is usually inconvenient since it requires the use of certain optical instruments. Accordingly, the present study proposed a new concept of combining the two parameters (C_D and “ a ”) into one single factor (C_{Da}). By obtaining the calibrated C_{Da} variation (Figure 6) as functions of the thickness (B) and volume ratio (γ) of the tree body, the computation of the resulting flow field is then ready to proceed. This is considered a major contribution of the present study.

8. Conclusions

A method of identifying the tree factor was proposed. By comparing with the measurement results of the velocity profiles downstream of rectangular tree panels,

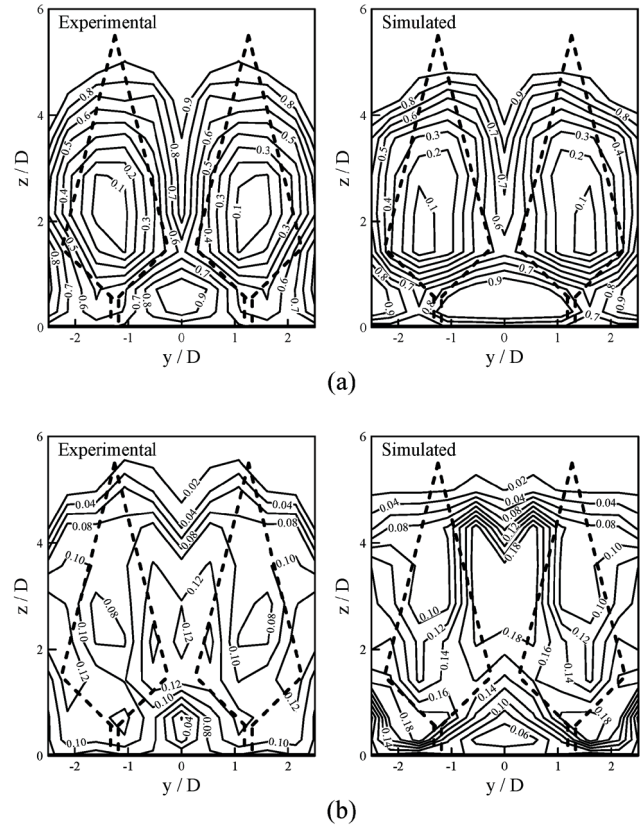


Figure 12. Comparison of velocity profiles of dual trees in a side-by-side arrangement ($x_D = 8D$).

the C_{Da} value associated with the thickness (B) and volume ratio (γ) of the tree body was calibrated numerically by a try-and-error procedure. Accordingly, the variation of C_{Da} in relation to B and γ was proposed.

The variation of the volumetric tree ratio (γ) should cover the range of general engineering applications regarding broad-leaf trees. The validity range of B , however, is limited up to 0.70 m. To simulate flows past a broad-leaf tree with a greater horizontal thickness, an extended study is suggested in the future to find out the C_{Da} variation with a larger range of the horizontal tree thickness.

Based on the calibrated contour plot of C_{Da} , simulations of uniform flows past an isolated tree, and dual trees in a tandem and a side-by-side arrangement were performed to examine the validity of the numerical method. The comparisons, in terms of the downstream mean and root-mean-square velocity profiles, indicated that the flows were well predicted.

Finally, as the sway motion of trees can be neglected, it is concluded that the calibrated variation of C_{Da} can be readily employed to simulate flows past discrete broad-leaf trees with adequate accuracy.

Acknowledgement

The study was cordially sponsored by National Science Council in Taiwan (Grant No. NSC 102-2221-E-005-058).

References

- [1] Finnigan, J., "Turbulence in Plant Canopies," *Annual Review of Fluid Mechanics*, Vol. 32, pp. 519–571 (2000). doi: [10.1146/annurev.fluid.32.1.519](https://doi.org/10.1146/annurev.fluid.32.1.519)
- [2] Raupach, M. R., Antonia, R. A. and Rajagopalan, S., "Rough-Wall Turbulent Boundary Layers," *Applied Mechanics Reviews*, Vol. 44, pp. 1–25 (1991). doi: [10.1115/1.3119492](https://doi.org/10.1115/1.3119492)
- [3] Raupach, M. R., Coppin, P. A. and Legg, B. J., "Experiments on Scalar Dispersion within a Model Plant Canopy. Part I: the Turbulence Structure," *Boundary-Layer Meteorology*, Vol. 35, pp. 21–52 (1986). doi: [10.1007/BF00117300](https://doi.org/10.1007/BF00117300)
- [4] Mihailovic, D. T., Lalic, B., Rajkovic, B. and Arsenic, I., "A Roughness Sublayer Wind Profile above Non-Uniform Surface," *Boundary-Layer Meteorology*, Vol. 93, pp. 425–451 (1999). doi: [10.1023/A:1002063405979](https://doi.org/10.1023/A:1002063405979)
- [5] Massman, W., "A Comparative Study of some Mathematical Models of the Mean Wind Structure and Aerodynamic Drag of Plant Canopies," *Boundary-Layer Meteorology*, Vol. 40, pp. 179–197 (1987). doi: [10.1007/BF00140075](https://doi.org/10.1007/BF00140075)
- [6] Novak, M. D., Warland, J. S., Orchaansky, A. L., Ketler, R. and Green, R., "Wind Tunnel and Field Measurements of Turbulent Flow in Forests, Part I: Uniformly Thinned Stands," *Boundary-Layer Meteorology*, Vol. 95, pp. 457–495 (2000). doi: [10.1023/A:1002693625637](https://doi.org/10.1023/A:1002693625637)
- [7] Boldes, U., Colman, J. and Maranon, D. L. J., "Field Study of the Flow Behind Single and Double Row Herbaceous Windbreaks," *Journal of Wind Engineering and Industrial Aerodynamics*, Vol. 89, pp. 665–687 (2001). doi: [10.1016/S0167-6105\(01\)00065-4](https://doi.org/10.1016/S0167-6105(01)00065-4)
- [8] Flesch, T. K. and Wilson, J. D., "Wind and Remnant Tree Sway in Forest Cutblocks. I. Measured Winds in Experimental Cutblocks," *Agricultural Forest Meteorology*, Vol. 93, pp. 229–242 (1999). doi: [10.1016/S0168-1923\(98\)00112-9](https://doi.org/10.1016/S0168-1923(98)00112-9)
- [9] Flesch, T. K. and Wilson, J. D., "Wind and Remnant Tree Sway in Forest Cutblocks. II. Relating Measured Tree Sway to Wind Statistics," *Agricultural Forest Meteorology*, Vol. 93, pp. 243–258 (1999). doi: [10.1016/S0168-1923\(98\)00113-0](https://doi.org/10.1016/S0168-1923(98)00113-0)
- [10] Shaw, R. H. and Schumann, U., "Large-eddy Simulation of Turbulent Flow above and within a Forest," *Boundary-Layer Meteorology*, Vol. 61, pp. 47–64 (1992). doi: [10.1007/BF02033994](https://doi.org/10.1007/BF02033994)
- [11] Wilson, J. D. and Flesch, T. K., "Wind and Remnant Tree Sway in Forest Cutblocks. III. A Windflow Model to Diagnose Spatial Variation," *Agricultural Forest Meteorology*, Vol. 93, pp. 259–282 (1999). doi: [10.1016/S0168-1923\(98\)00121-X](https://doi.org/10.1016/S0168-1923(98)00121-X)
- [12] Su, H. B., Shaw, R. H., Pawu, K. T., Moeng, C. H. and Sullivan, P. P., "Turbulent Statistics of Neutrally Stratified Flow Within and above a Sparse Forest from Large-Eddy Simulation and Field Observations," *Boundary-Layer Meteorology*, Vol. 88, pp. 363–397 (1998). doi: [10.1023/A:1001108411184](https://doi.org/10.1023/A:1001108411184)
- [13] Patton, E. G. and Davis, K. J., "Decaying Scalars Emitted by a Forest Canopy: a Numerical Study," *Boundary-Layer Meteorology*, Vol. 100, pp. 91–129 (2001). doi: [10.1023/A:1019223515444](https://doi.org/10.1023/A:1019223515444)
- [14] Watanabe, T., "Large Eddy Simulation of Coherent Turbulence Structures Associated with Scalar Ramps over Plant Canopies," *Boundary-Layer Meteorology*, Vol. 112, pp. 307–341 (2004). doi: [10.1023/B:BOUN.0000027912.84492.54](https://doi.org/10.1023/B:BOUN.0000027912.84492.54)
- [15] Sládek, I., Bodnar, T. and Kozel, K., "On a Numerical Study of Atmospheric 2D and 3D-Flows over a Complex Topography with Forest Including Pollution Dispersion," *Journal of Wind Engineering and Industrial*

- Aerodynamics*, Vol. 95, pp. 1424–1444 (2007). doi: [10.1016/j.jweia.2007.02.024](https://doi.org/10.1016/j.jweia.2007.02.024)
- [16] Song, C. C. S. and Yuan, M., “A Weakly Compressible Flow Model and Rapid Convergence Methods,” *ASME Journal of Fluids Engineering*, Vol. 110, pp. 441–455 (1988). doi: [10.1115/1.3243575](https://doi.org/10.1115/1.3243575)
- [17] Smagorinsky, J., “General Circulation Experiments with Primitive Equations,” *Monthly Weather Review*, Vol. 91, pp. 99–164 (1963). doi: [10.1175/1520-0493\(1963\)091<0099:GCEWTP>2.3.CO;2](https://doi.org/10.1175/1520-0493(1963)091<0099:GCEWTP>2.3.CO;2)

Manuscript Received: Jan. 6, 2016

Accepted: Jul. 4, 2016